Pivotal Role of Gly 121 in Dihydrofolate Reductase from *Escherichia coli*: The Altered Structure of a Mutant Enzyme May Form the Basis of Its Diminished Catalytic Performance†

Richard S. Swanwick, Paul J. Shrimpton, and Rudolf K. Allemann*

School of Chemistry, University of Birmingham, Edgbaston, Birmingham B15 2TT, U.K.

Received December 2, 2003; Revised Manuscript Received January 16, 2004

ABSTRACT: The structure and folding of dihydrofolate reductase (DHFR) from *Escherichia coli* and the mutant G121V-DHFR, in which glycine 121 in the exterior FG loop was replaced with valine, were studied by molecular dynamics simulations and CD and fluorescence spectroscopy. The importance of residue 121 for the chemical step during DHFR catalysis had been demonstrated previously. High-temperature MD simulations indicated that while DHFR and G121V-DHFR followed similar unfolding pathways, the strong contacts between the M20 loop and the FG loop in DHFR were less stable in the mutant. These contacts have been proposed to be involved in a coupled network of interactions that influence the protein dynamics and promote catalysis [Benkovic, S. J., and Hammes-Schiffer, S. (2003) *Science 301*, 1196−1202]. CD spectroscopy of DHFR and G121V-DHFR indicated that the two proteins existed in different conformations at room temperature. While the thermally induced unfolding of DHFR was highly cooperative with a midpoint at 51.6 ± 0.7 °C, G121V-DHFR exhibited a gradual decrease in its level of secondary structure without a clear melting temperature. Temperature-induced unfolding and renaturation from the urea-denatured state revealed that both proteins folded via highly fluorescent intermediates. The formation of these intermediates occurred with relaxation times of 149 ± 4.5 and 256 ± 13 ms for DHFR and G121V-DHFR, respectively. The fluorescence intensity for the intermediates formed during refolding of G121V-DHFR was approximately twice that of the wild-type. While the fluorescence intensity then slowly decayed for DHFR toward a state representing the native protein, G121V-DHFR appeared to be trapped in a highly fluorescent state. These results suggest that the reduced catalytic activity of G121V-DHFR is the consequence of nonlocal structural effects that may result in a perturbation of the network of promoting motions.

The ubiquitous enzyme dihydrofolate reductase (DHFR)[1] is responsible for maintaining the intracellular pool of 5,6,7,8-tetrahydrofolate (H_4F) in prokaryotes and eukaryotes via the nicotinamide adenine dinucleotide phosphate (NADPH)-dependent reduction of 7,8-dihydrofolate (H_2F). H_4F is required for the biosynthesis of thymidylate, purines, and several amino acids (*1*), making DHFR an important pharmacological target. DHFR has been studied extensively by X-ray crystallography (*2*−*5*), NMR spectroscopy (*6*−*10*), and computation (*11*−*24*). DHFR from *Escherichia coli* is a monomeric enzyme consisting of four α-helices, eight β-sheets, and four mobile loops. The enzyme is separated into two domains, the adenosine binding domain (ABD) and the loop domain (LD) (Figure 1). High-temperature molecular dynamics (MD) simulations of the unfolding of DHFR suggested that the core of the LD and the N-terminal β-sheet (β1) form first followed by the folding of the ABD (*25*, *26*).

Previous studies have reported the central role of the M20, FG, and GH loops for the catalytic activity and mechanism of DHFR (Figure 1) (*27*). The M20 loop adopts the closed conformation in the reactive ternary complex when both H_2F and NADPH are bound (*5*). This conformation is stabilized through hydrogen bonds between residues in the M20 and FG loops. The backbone nitrogen atoms of these loops displayed high dynamic mobility in NMR relaxation experiments (*6*, *10*), which has been interpreted to suggest a connection between the dynamic properties of these loops and the catalytic behavior of DHFR. The relationship between movements of these loops and catalysis has been probed by site-directed mutagenesis. Replacement of Gly 121, a highly mobile residue located in the middle of the FG loop more than 19 Å from the active site (*6*, *10*), with Val or Leu slowed hydride transfer dramatically and weakened binding of NADPH (*28*). While being strictly conserved in all prokaryotic DHFRs, Gly 121 does not appear to form any interactions with other residues.

Molecular dynamics (MD) simulations of *E. coli* DHFR revealed a strong correlation between the movement of the catalytically important M20 and FG loops (*15*). These

† The financial support of the BBSRC and the University of Birmingham is gratefully acknowledged.

* To whom correspondence should be addressed. Telephone: 0121-414 4359. Fax: 0121-414 7871. E-mail: r.k.allemann@bham.ac.uk.

[1] Abbreviations: ABD, adenosine binding domain; CD, circular dichroism; DEAE, diethylaminoethane; DHFR, dihydrofolate reductase; H_4F, 5,6,7,8-tetrahydrofolate; H_2F, 7,8-dihydrofolate; LD, loop domain; MD, molecular dynamics; NADPH, reduced nicotinamide adenine dinucleotide phosphate; $NADP^+$, oxidized nicotinamide adenine dinucleotide phosphate; rmsd, root-mean-square deviation; Tris, tris-(hydroxymethyl)aminomethane.

10.1021/bi036164k CCC: $27.50
Published on Web 03/16/2004

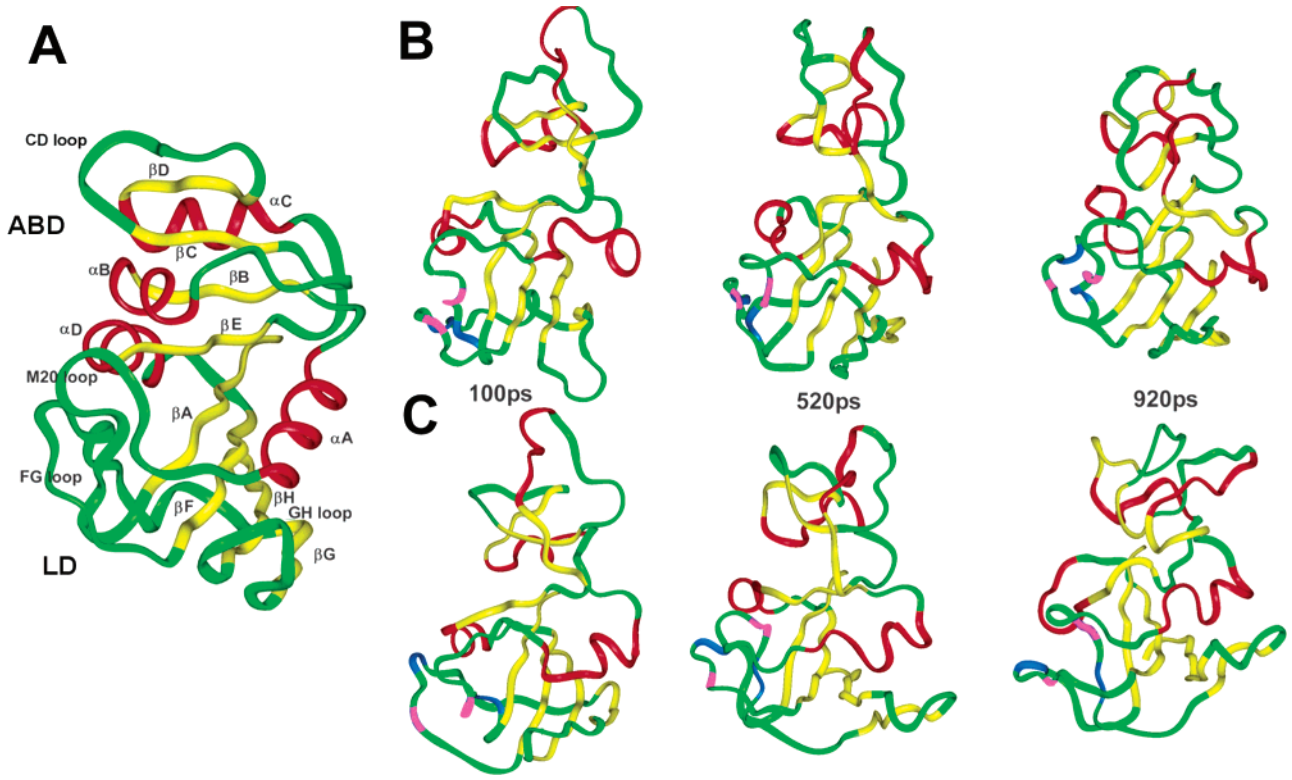

FIGURE 1: (A) Structure of *E. coli* DHFR taken from PDB entry 1RX2 showing α-helices in red, *β*-strands in yellow, and loops and random coils in green. Secondary structure elements mentioned in the text are indicated. Snapshot structures from typical DHFR (B) and G121V-DHFR (C) simulations at 500 K at 100, 520, and 920 ps. The structures are colored according to the secondary structural characteristics from the X-ray structure. Residues 12, 13, 124, and 125, which are involved in three of the native contacts (light blue), and residues 15, 16, and 121, which are involved in the two other native contacts between the M20 and FG loops (pink), are also shown.

correlated motions were only observed in reactive complexes of the enzyme and were absent in the product complex. Mixed quantum mechanical molecular mechanics (QM/MM) simulations and genomic sequence analysis have identified a network of hydrogen bonds and van der Waals contacts from Asp 122 on the surface of the protein to the active site (*14*). This network may facilitate hydride transfer (*29*), suggesting a direct link between the motion of the FG loop and the catalytic events in the active site. In good agreement with the kinetic measurements, computation revealed a significant increase in the energy barrier for the hydride transfer of the Gly 121 to Val mutant (G121V-DHFR) relative to the wild-type enzyme (DHFR) (*13*). Because no X-ray structure for G121V-DHFR was available, the structure of the mutant enzyme was generated by building the valine side chain onto the glycine backbone of the wild-type structure (*13*). Rotamer libraries were then used to determine the most likely orientation of the isopropyl side chain followed by a full equilibration of the entire system prior to data collection in an unrestrained calculation. This is a reasonable procedure as in the majority of cases structural changes arising from point mutations are limited to the conformation of side chain of the mutated residue and those side chains contacting it (*30*−*33*). However, the above observation was based on analysis of crystal structures of mutants. Since there is to date no such structure for G121V-DHFR, we have used both theoretical and experimental techniques to investigate the relative stabilities and folding properties of DHFR and G121V-DHFR.

High-temperature MD simulations for investigating the unfolding of DHFR and G121V-DHFR revealed significant differences in the stability of the tertiary structural elements surrounding the site of the mutation. Stopped-flow fluorescence and CD spectroscopy confirmed that the structural and folding properties of the mutant were different from those of the wild-type enzyme. These results demonstrate that the primary sequence of the FG loop of DHFR plays an important role in atomic packing and/or protein dynamics with consequences for the tertiary structure, stability, and functional activity of the whole protein.

MATERIALS AND METHODS

Biochemicals. All reagents were molecular biology-grade and from Sigma. Diethylaminoethane fast flow (DEAE) ion-exchange resin, methotrexate−agarose, and DEAE-Sepharose were from Amersham Biosciences and Sigma, respectively. All enzymes required for recombinant DNA methods were obtained from New England Biolabs.

Computation. Procedures similar to those described previously were used (*26*). All simulations were carried out using the c28b1 version of CHARMM (*34*). Effective Energy Function 1 (*35*) represented solvent. The CHARMM 19 polar hydrogen energy function (*36*) was used to describe the protein (*26*, *37*). For a more detailed description of the suitability of the method, see ref *26*. Initial protein coordinates were taken from a ternary complex of the enzyme with folate and $NADP^+$ [PDB entry 1RX2 (*5*)]. The coordinates for folate, the cofactor, and all crystallographic waters were deleted.

Wild-Type Control Simulation. After 1000 steps of Adopted Basis Newton−Raphson (ABNR) minimization, the protein

was heated to 300 K over the course of 10 ps followed by a 20 ps equilibration. The final structure from the minimization and heating procedure was then used as the starting point for a 1 ns control simulation at 300 K. A 2 fs time step was used, and coordinates were saved every 2 ps. The Verlet leapfrog algorithm was used for all MD simulations.

Wild-Type High-Temperature Simulations. Twenty 1 ns simulations were carried out at 500 K. The starting points for each were structures taken at regular intervals from the control simulation described above. Each was, after a short minimization (500 steps of ABNR), heated to 500 K over the course of 20 ps before a production run at 500 K for 1 ns. A 2 fs time step was used, and coordinates were saved every 2 ps.

Mutant Enzyme High-Temperature Simulations. The 20 structures obtained from the wild-type control simulation were modified to build the Val side chain onto the backbone of Gly 121 using InsightII (Biosym Technologies Inc., San Diego, CA). Each time, the Cα−Cβ torsion was set so that the Cγ atoms were in one of the three possible staggered configurations relative to the backbone nitrogen and carbonyl groups. This meant that of the three possible configurations, two were used as starting structures seven times and the other was used six times. Each of these mutant structures was then subjected to a 1 ns simulation at 500 K as described above.

Analysis. Moil-view (version 10.1) (*38*) was used to calculate root-mean-square deviations (rmsds), to measure interatomic distances, and for visual analysis of the trajectories. The control simulation was analyzed for native contacts that were described as any two nonconsecutive Cα atoms that were less than 6 Å apart for ≥70% of the simulation. This definition is the same as that used previously (*26*). All native contacts found in the control simulation were then monitored in the high-temperature trajectories.

Cloning of the DNA for DHFR and Site-Directed Mutagenesis. Wild-type *E. coli* DHFR was amplified from *E. coli* genomic DNA using standard PCR techniques. The forward primer (5′-GAGGCACATATGATCAGTCTGATTGCGGCG-3′) introduced an *Nde*I restriction site, and the reverse primer (5′-CTCAGCGGATCCTTATTACCGCCGCTCCAGAATCTC-3′) introduced a *Bam*HI restriction site. The PCR product was purified by agarose gel electrophoresis and digested with *Nde*I and *Bam*HI, and the resulting fragment was inserted into pET21a (Novagen).

G121V-DHFR was generated using the QuikChange site-directed mutagensis kit (Stratagene) following the manufacturer's protocol. Mutagenic primers were 5′-CGACGCAGAAGTGGAAGTCGACACCCATTTCCCG-3′ and 5′-CGGGAAAATGGGTGTCGACTTCCACTTCTGCGTCG-3′ (mutations are underlined). DNA sequences were confirmed by automated DNA sequencing (Functional Genomics Laboratory, School of Biosciences, University of Birmingham).

Protein Purification. For the production of DHFR and G121V-DHFR, BL21(DE3) cells containing the respective plasmid were grown at 37 °C in LB medium containing 200 μg/mL ampicillin to an OD_{600} of 0.8. Isopropyl β-D-thiogalactoside was added to a final concentration of 0.4 mM, and the cells were grown for an additional 4 h. Cells were harvested by centrifugation (3000*g* for 30 min), resuspended in 25 mM sodium phosphate (pH 7.0) and 5 mM EDTA, and sonicated for 5 min on ice. The lysate was cleared by centrifugation (50000*g* for 30 min). The supernatant was applied to a methotrexate−agarose column (10 mL), which had been pre-equilibrated with 25 mM sodium phosphate (pH 7.0), 250 mM NaCl, and 5 mM EDTA. The column was washed with 200 mL of the same buffer followed by elution of bound proteins with 25 mM sodium phosphate (pH 7.0), 250 mM NaCl, and 5 mM EDTA containing 2 mM folate. The eluted protein was dialyzed for 24 h against three changes of 2 L of 10 mM potassium phosphate (pH 7), 0.2 mM EDTA, and 1 mM 2-mercaptoethanol. The dialysate was applied to DEAE-Sepharose (15 mL) equilibrated with 25 mM Tris (pH 8.0) and 5 mM EDTA. Bound proteins were eluted with a gradient from 0 to 1 M NaCl in 25 mM Tris (pH 8.0), 5 mM EDTA, and 1 mM 2-mercaptoethanol, affording essentially pure protein as judged by SDS gel electrophoresis. Protein concentrations were determined spectroscopically assuming an extinction coefficient of 3.11×10^4 M^{-1} cm^{-1} at 280 nm and by titration with methotrexate (*39*). Turnover numbers for DHFR and G121V-DHFR were in good agreement with those previously reported (*28*, *39*).

CD and Fluorescence Spectroscopy. Equilibrium and kinetic measurements were carried out in 10 mM potassium phosphate (pH 7.0), 0.2 mM EDTA, and 1 mM 2-mercaptoethanol with a protein concentration of 10 μM. CD spectra (J-810 CD spectropolarimeter, Jasco) were obtained by scanning from 190 to 260 nm, with a 0.5 nm pitch using a stepped wavelength response of 1 s and a bandwidth of 2 nm. CD unfolding measurements were obtained with temperature increments of 10 °C and temperature slopes of 0.5 °C/s. Mean residue ellipticities ($[\theta]_R$) were calculated using the formula $[\theta]_R = [\theta]/[10(n - 1)cl]$, where $[\theta]$ is the measured ellipticity in millidegrees, n is the number of amide bonds, c is the concentration in molar, and l is the path length in centimeters. All reported values of $[\theta]_R$ are the average of four independent experiments, and the standard errors are indicated for 1σ.

Fluorescence unfolding was monitored using an LS-55 luminescence spectrometer (Perkin-Elmer) fitted with a temperature-controlled cuvette holder with a path length of 10 mm and slit widths of 2.5 nm. Excitation and emission wavelengths were 292 and 340 nm, respectively. Temperature increments of 1 °C were followed by an equilibrium period of 2 min before measurement. The concentrations of the proteins were 10 μM.

Kinetic refolding experiments were carried out at 25 °C using an SX 18MV-R stopped-flow spectrometer (Applied Photophysics) in the fluorescence mode. The dead time of the instrument was 2.5 ms in a cell with a path length of 2 mm. The refolding reaction was initiated by a concentration jump from 8 to 0.8 M urea using a 1:10 mixing ratio. The protein concentration after mixing was 10 μM. DHFR had been shown to resist denaturation by urea for concentrations up to 2 M (*40*). Conformational changes were monitored using an excitation wavelength of 292 nm and measuring the intensity of the fluorescence with a cutoff filter (>320 nm) with entrance and exit slit widths of 1 mm. Data were collected with a single time base (1000 data points) over the course of 10 s.

RESULTS

Control MD Simulation at 300 K. The reduction in the catalytic activity of *E. coli* DHFR caused by the substitution

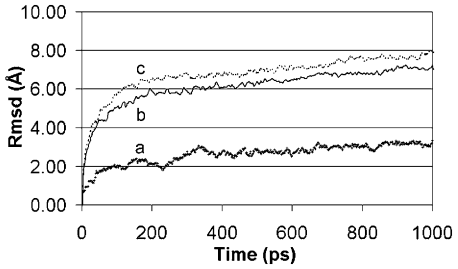

FIGURE 2: Root-mean-square deviations (rmsds) of all the Cα atoms vs time for the 300 K control simulation (a), the average of 20 simulations at 500 K each for DHFR (b), and G121V-DHFR (c).

of Gly 121 with Val has been the focus of much recent interest (*13*−*15*, *27*−*29*, *41*). As there is currently no structure of the mutant G121V-DHFR, computational studies have been based on the assumption that its backbone structure was similar to that of the wild-type enzyme. High-temperature MD simulations of the folding pathways of various enzymes (*37*, *42*−*47*), including *E. coli* DHFR (*26*), have generally shown good agreement with experimental studies. Here we report the results from a series of MD simulations of both DHFR and G121V-DHFR at high temperatures for studying further the effects of the mutation of Gly 121 in *E. coli* DHFR.

A control simulation of DHFR was carried out at a temperature of 300 K to benchmark the high-temperature simulations. The rmsd of all the Cα atoms showed that the simulation was stable (Figure 2), indicating that the DHFR fold observed in the crystal structure was maintained during the simulation. Secondary and tertiary structure elements were analyzed by the identification of native contacts, which were defined where two nonsequential Cα atoms were within 6 Å of each other in at least 70% of the frames of the simulation (*26*). This led to the identification of 145 native contacts for a 1 ns simulation of DHFR at 300 K (Figure 3A), in good agreement with a previous study of the wild-type enzyme (*26*).

Unfolding MD Simulations at 500 K. The potential unfolding of both DHFR and G121V-DHFR was addressed in 40 MD 1 ns simulations at 500 K. The DHFR simulations were started from structures obtained at regular intervals from the 300 K simulation, and the results were in general agreement with those previously reported (*26*). For the G121V-DHFR simulations, the 20 DHFR structures were modified to generate a structure for the mutant as described in Materials and Methods. A separate control simulation for the mutant was not performed as previous work had shown that, within the confines of an MD simulation at 300 K, the mutant G121V-DHFR behaved like wild-type DHFR (P. J. Shrimpton and R. K. Allemann, unpublished results). Only minor deviations of the backbone atoms from the starting structure were observed during these simulations.

The average rmsd of all the Cα atoms versus time of all 20 DHFR simulations showed a maximum of 7.2 Å (Figure 2), lower than the value of 13 Å seen previously (*26*). The average rmsd of the Cα atoms of G121V-DHFR versus time for all 20 simulations was found to be slightly higher than for the wild-type, peaking at 8.0 Å (Figure 2). However, analysis of each individual rmsd plot showed that this increase was not a significant result. Both forms of the enzyme had significantly higher Cα rmsd values at 500 K than had been observed in the control simulation at 300 K (Figure 2). However, all simulations showed the presence of some residual secondary or tertiary structure. Analysis showed that not all trajectories behaved the same but that general trends could be formed.

As expected from the rmsd plots (Figure 2), both the wild-type and mutant enzymes showed similar behavior at 500 K. The first contacts lost were usually in the ABD, normally those between β-strand B and strands C and E, followed by loss of interactions between β-strands C and D (Figure 1). After the loss of these initial contacts, α-helices B and to a lesser extent C began to unfold. Contacts between residues i and $i + 3$ in the helices were usually lost before the $i-i+2$ interactions. After the tertiary contacts between β-sheets B and E were lost completely, helix A unfolded, again losing first the interactions between residues i and $i + 3$. Interestingly, the contacts between the CD loop and strand D were seen to be much more stable than the intersheet contacts. Later unfolding events were the loss of the contacts between β-strands A and E as the ABD became completely unfolded. This was normally associated with the beginning of the loss of structure within helix D. The most stable contacts, across all the simulations, were those between β-strands A and F in the core of the LD.

In the majority of DHFR simulations, contacts between the M20 loop and the FG loop were stable until late stages. In some cases, these contacts remained formed throughout the whole trajectory. In 20% of DHFR simulations, these contacts were lost early with the subsequent loss of structure in β-strands F and then G and associated loss of contacts between these strands and also with strand H.

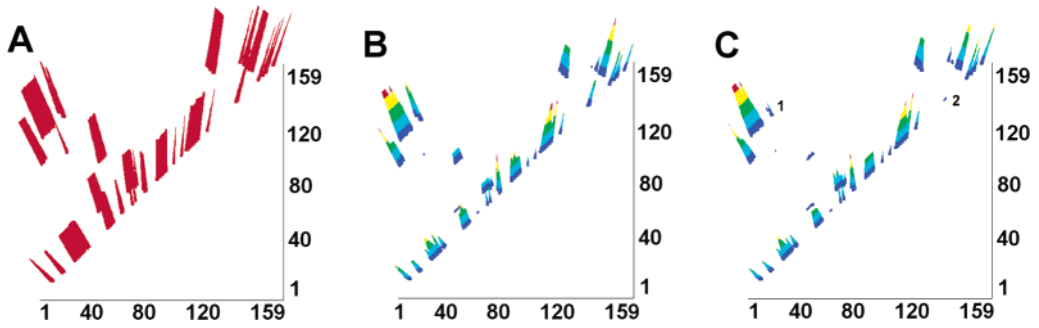

FIGURE 3: (A) Map of the 145 native contacts (as defined in the text) identified during a 1 ns MD simulation of DHFR at 300 K. Average occurrence of each of the 145 native contacts for 20 DHFR (B) and 20 G121V-DHFR (C) simulations at 500 K. The color indicates the percentage of time that each contact was intact: red for >80%, yellow for 61−80%, green for 41−60%, light blue for 21−40%, and dark blue for <20%. The contacts between the M20 and FG loops (1) and the local contacts within the FG loop (2) are highlighted for G121V-DHFR.

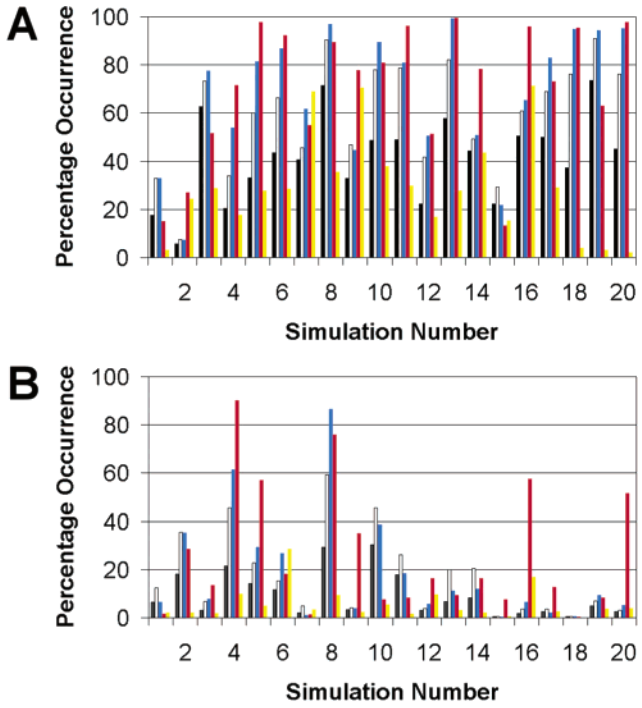

FIGURE 4: Percentage occurrence during 500 K MD simulations of the five native contacts between the M20 loop and FG loop for each of the 20 DHFR simulations (A) and the 20 G121V-DHFR simulations (B). Contacts between residues 12 and 124 are shown in black, between residues 12 and 125 in white, between residues 13 and 125 in blue, between residues 15 and 121 in red, and between residues 16 and 121 in yellow.

The occurrences of all 145 native contacts identified from the 300 K trajectory were monitored throughout each of the high-temperature simulations. Average native contact maps were produced for DHFR (Figure 3B) and G121V-DHFR (Figure 3C). Analysis of each individual run showed that it was rare for contacts to be lost and then re-formed and that the majority of simulations exhibited similar patterns. Therefore, the contacts with the lowest average occurrences were generally assumed to be those lost earliest in the unfolding process.

Comparison of the contact maps of DHFR and G121V-DHFR showed one major difference, namely, that the contacts between the M20 and FG loops and the local contacts within the FG loop occurred much less frequently in the mutant (Figures 3 and 4). Interestingly, the contacts between β-strands G and H and in the GH loop, C-terminal to the FG loop, were similar for the two enzymes, as were other interactions with the M20 loop and β-strand F (Figure 3). When the five native contacts between the M20 loop and the FG loop seen in the control simulation were plotted for each of the 20 simulations of DHFR and G121V-DHFR, it was clear that they were less stable in the mutant (Figure 4). While they were lost early in the unfolding process in four of the DHFR simulations (Figure 4A), they were lost in 16 of the G121V-DHFR simulations (Figure 4B). The simulations of DHFR and G121V-DHFR were started from the same initial structure, with the exception of the side chain of residue 121. Therefore, the different stabilities in the region of the contacts between the M20 and FG loops observed may indicate either a late folding event in G121V-DHFR or the formation of a different native structure.

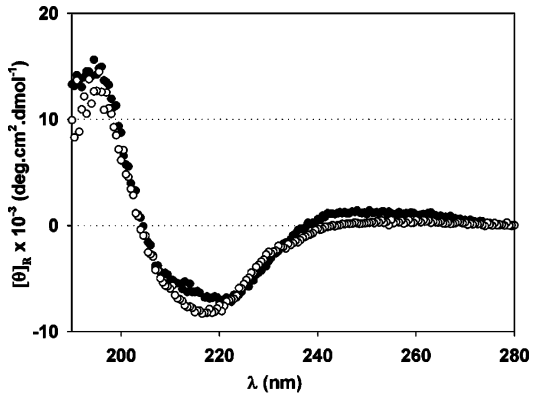

FIGURE 5: Far-UV CD spectra of DHFR (○) and G121V-DHFR (●) between 190 and 280 nm at 20 °C. The protein concentration was 10 μM in 10 mM potassium phosphate (pH 7), 0.2 mM EDTA, and 1 mM 2-mercaptoethanol.

Structural Characterization of the DHFR and G121V-DHFR by CD Spectroscopy. The computational results described above suggested the existence of nonlocal differences in the structural and folding properties of DHFR and G121V-DHFR, which could be studied experimentally. DHFR and G121V-DHFR were therefore produced in BL21-(DE3) cells and purified to homogeneity according to well-established protocols by affinity chromatography on methotrexate−agarose and anion-exchange chromatography.

The far-UV CD spectra of DHFR and G121V-DHFR were different (Figure 5). The spectrum of the wild-type enzyme had a single minimum at 218 nm and a maximum at 195 nm. The mean residue ellipticity at 218 nm was -9150 ± 330 deg cm^2 dmol^{-1}, which compared well with the published value (*40*, *48*, *49*). This minimum was shifted to 222 nm for G121V-DHFR and its intensity reduced to -7450 ± 375 deg cm^2 dmol^{-1}, indicating that the secondary structures of the two proteins were slightly different. The addition of cofactor or substrate did not significantly change the CD spectrum of G121V-DHFR.

The thermal stabilities of DHFR and G121V-DHFR were determined by measuring CD spectra at various temperatures (Figure 6). An isodichroic point was identified at 230 nm for both proteins. Further isodichroic points were identified at 211.5 and 215 nm for the wild-type and the mutant, respectively. The thermal unfolding profile of DHFR at 222 nm exhibited small linear variations of the signal between 20 and 40 °C corresponding to native baselines with a sharp cooperative unfolding reaction and unfolded baseline regions at temperatures greater than 64 °C (Figure 6A). The midpoint of the transition was at 51.6 ± 0.7 °C. In contrast, G121V-DHFR did not exhibit this highly cooperative unfolding behavior, but rather, a gradual decrease in mean residue ellipticity at 222 nm was observed (Figure 6B); therefore, no melting temperature could be determined for the mutant. The spectra of both proteins at high temperatures were identical (Figure 6), indicating identical states under these conditions. The mean residue ellipticity at 222 nm of -5095 ± 215 deg cm^2 dmol^{-1} indicated that some residual secondary structure was present in the thermally unfolded forms.

Thermal Unfolding of DHFR and G121V-DHFR by Fluorescence Spectroscopy. The thermal unfolding reactions of DHFR and G121V-DHFR were also monitored by fluorescence spectroscopy. The temperature dependence of

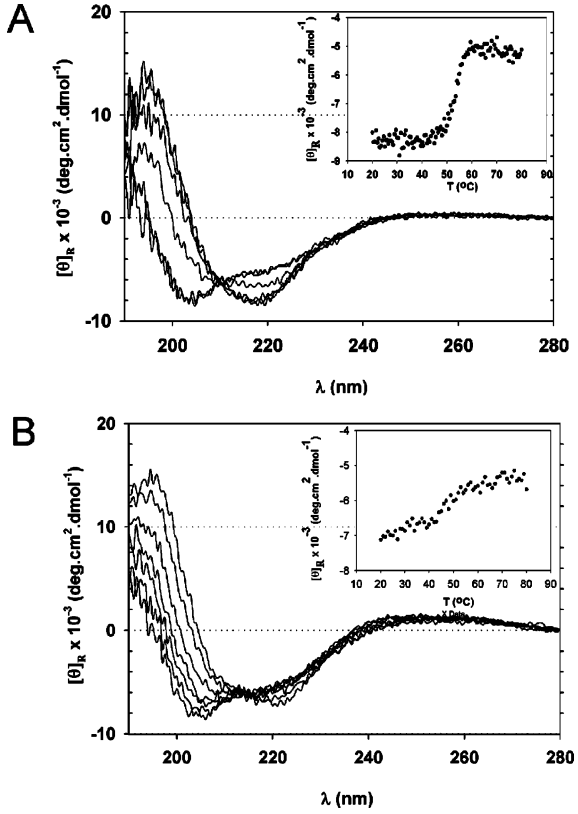

FIGURE 6: Temperature dependence of the far-UV CD spectra of DHFR (A) and G121V-DHFR (B) between 190 and 280 nm between 20 and 80 °C for temperature increments of 10 °C. The insets depict mean residue ellipticities at 222 nm for DHFR (A) and G121V-DHFR (B) as a function of temperature. The protein concentrations were 10 μM in 10 mM potassium phosphate (pH 7), 0.2 mM EDTA, and 1 mM 2-mercaptoethanol.

the fluorescence signal at 340 nm of DHFR revealed major structural changes around 51 °C, which corresponded to the melting temperature of the enzyme as determined in CD experiments (*vide supra*) (Figure 7A). The disruption of structure appeared to occur in two stages. First, an approximately 28% increase in the fluorescence intensity occurred with a midpoint at ~43 °C followed by a rapid decrease of the fluorescence intensity above 51 °C toward the unfolded state. These results indicated that at least one intermediate existed in the thermal unfolding of DHFR as had been described previously (*49*, *50*).

The fluorescence intensity of G121V-DHFR at ambient temperature was approximately 33% higher than that of the wild-type enzyme at the same temperature (Figure 7A). Its fluorescence was however only 12% higher than that of the highly fluorescent state of DHFR. With increasing temperatures up to approximately 46 °C, the magnitude of the fluorescence signal for G121V-DHFR diminished only slightly. At higher temperatures, a rapid decrease in the intensity of the fluorescence signal was observed, similar to that observed for DHFR.

Refolding Kinetics of DHFR and G121V-DHFR. Refolding of DHFR from the denatured state has been described to occur via the population of two classes of intermediates. First, a marginally stable burst phase intermediate is formed, which is characterized by a high degree of secondary structure and an exposed hydrophobic core (*51*, *52*), followed by the formation of an ensemble of metastable species, designated

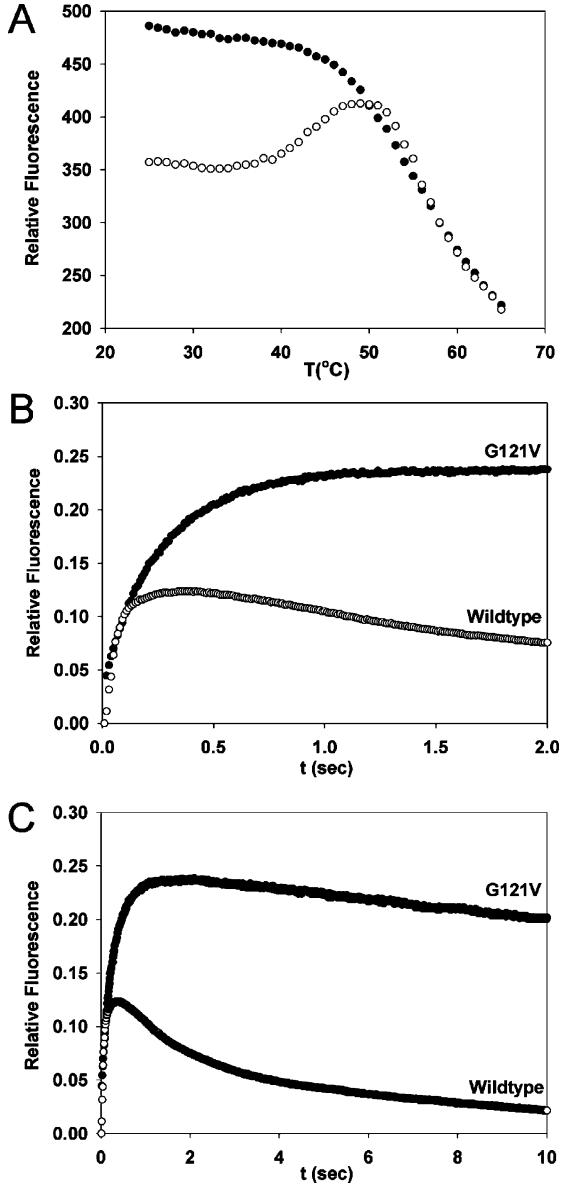

FIGURE 7: Folding and unfolding of DHFR and G121V-DHFR measured by fluorescence spectroscopy. (A) Thermal unfolding of DHFR (○) and G121V-DHFR (●) measured by fluorescence. The protein concentrations were 10 μM in 10 mM potassium phosphate (pH 7), 0.2 mM EDTA, and 1 mM 2-mercaptoethanol. Plots of the change in the relative fluorescence intensity of DHFR and G121V-DHFR as a function of time from 0 to 2 s (B) and from 0 to 10 s (C) for a refolding jump from 8 to 0.8 M urea at 25 °C. The final protein concentrations were 10 μM in 10 mM potassium phosphate (pH 7), 0.2 mM EDTA, and 1 mM 2-mercaptoethanol.

as the highly fluorescent intermediate(s), which contains specific tertiary structure (*53*). The above results from thermal unfolding suggested therefore that at low temperatures the mutant enzyme adopted a conformation similar to that of the highly fluorescent folding intermediate of the wild-type.

The formation of the highly fluorescent intermediate(s) was monitored by stopped-flow fluorescence. The relative fluorescence intensity as a function of time was measured for refolding jumps from 8 to 0.8 M urea for DHFR and G121V-DHFR (Figure 7B). The fluorescence signal for DHFR rapidly rose to its maximal value with a relaxation time of 149 ± 4.5 ms, followed by a slow decrease in intensity leading to the formation of the native fold. This

behavior was in good agreement with previous reports (*54*, *55*) and indicative of the transient population of a highly fluorescent intermediate followed by the formation of the native protein.

Similar to the behavior of the wild-type enzyme, refolding of G121V-DHFR was accompanied by an increase in the intensity of the fluorescence signal. The relaxation time of 256 ± 13 ms was slightly longer than that measured for DHFR (Figure 7B). The maximal value in the intensity observed for G121V-DHFR was approximately twice that observed for DHFR. In contrast to the early folding events, the decay of the intermediate into the folded state was different for the mutant enzyme. While the highly fluorescent intermediate of DHFR decayed relatively rapidly to the folded state (*54*), the intermediate state observed for G121V-DHFR was much more stable, and only a slow decrease in the fluorescence intensity was observed (Figure 7B). The mutant protein appeared to be trapped at a point in the folding process that corresponded to a highly fluorescent intermediate. However, the different fluorescence intensities for the mutant and wild-type implied that there were structural differences between the two intermediate structures.

DISCUSSION

This report presents a combination of theoretical and experimental evidence suggesting that replacing Gly 121 with Val in the FG loop of DHFR results in a change in the folded structure of the mutant. Although Gly 121 is on the exterior of the protein and more than 12 Å from C4 of NADPH, kinetic work had indicated that its replacement resulted in a reduction in the rate of hydride transfer of more than 2 orders of magnitude (*28*). NMR relaxation experiments revealed that the backbone nitrogen atoms of residues in the FG loop were highly mobile (*6*, *10*). Molecular dynamics simulations identified a set of strongly coupled motions between the FG loop and the M20 loop (*15*), the conformation of which had been suggested to be important in the catalytic cycle (*5*). These correlated motions were only present in the reactive complex (DHFR·NADPH·H_2F) but were not observed in the product complex and were drastically diminished in G121V-DHFR (*41*). A network of interactions within DHFR was identified that might promote catalysis (*14*, *15*). Hammes-Schiffer and co-workers suggested that the replacement of Gly 121 with Val might interrupt this network of promoting motions, thereby reducing the catalytic activity of the enzyme (*13*). Such a direct coupling between enzyme dynamics and catalysis through a network of promoting motions (*29*) might explain how local structural changes could have long-range effects. Molecular mechanics simulations of DHFR and G121V-DHFR had, however, suggested that distal mutations can have structural effects on the active site, thereby providing an alternative explanation for their effect on catalysis (*41*). It may be surprising that the replacement of a residue situated in a loop on the outside of the protein may potentially have such structural effects. Examination of high-resolution structural data of DHFR indicated, however, that the isopropyl side chain introduced by the conversion of Gly to Val pointed toward the interior of the enzyme, potentially leading to unfavorable steric interactions with other residues in the interior of the enzyme.

The MD simulations of DHFR and G121V-DHFR reported here indicated that both the wild-type and the mutant, when stated from the same folded structure, followed similar pathways during temperature-induced unfolding. While there were slight differences in the detail of the events in the unfolding of DHFR observed here and those reported in a previous study (*26*), the same general conclusions were reached. For both DHFR and G121V-DHFR, an initial collapse of the ABD into more extended loops was followed by a gradual breakdown of the remaining β-sheet structure in the ABD (Figure 1). The LD was more stable and unfolded relatively late in the simulations.

The major differences between DHFR and G121V-DHFR were that the contacts between the M20 loop and the FG loop were lost much more readily in the mutant (Figures 3 and 4). Contacts between these two loops have been shown to be critical for the catalytic properties of DHFR. In the catalytically active, closed conformation, the NH group and the carboxylate of Asp 122 in the FG loop are hydrogen bonded to the carbonyl of Gly 15 and the NH group of Glu 17 in the M20 loop, while the oxygen in the side chain of Thr 123 forms a hydrogen bond to the NH group of Ile 14 (*5*). These bonds, which control the movement of the M20 loop between the closed and the occluded conformations, have been suggested to be involved in a network of promoting motions (*29*). MD 1 ns simulations of the ternary complex of G121V-DHFR with NADPH and H_2F at 300 K indicated that the hydrogen bonds between Asp 122 and Gly 15 and between Glu 17 and Asp 122 were broken (P. J. Shrimpton and R. K. Allemann, unpublished results). Similar observations have been reported by Brooks III and co-workers (*41*). Due to the nature of these simulations, the backbone atoms in the FG and M20 loops did not undergo significant conformational changes. The unfolding studies presented here suggested that the mutation of residue 121 of DHFR could not only generate subtle long-range perturbations in correlated (*15*, *41*) or promoting (*13*, *14*) motions but also lead to conformational changes involving rearrangements of backbone atoms with implications for the kinetic activity of the mutant. In this context, it is noteworthy that kinetic experiments for G121V-DHFR revealed a conformational change prior to the chemical step (*28*).

A comparison of the CD spectra of DHFR and G121V-DHFR indicated that the two proteins may adopt different conformational states at room temperature. While the spectra were similar in shape, the minimum in mean residue ellipticity observed was shifted from 218 nm for the wild-type to 222 nm in the mutant, together with a decrease in its intensity by almost 19% (Figure 5). The thermal unfolding reaction of DHFR occurred in a highly cooperative fashion with a melting point of approximately 52 °C (Figure 6A). On the other hand, a gradual increase with temperature of the mean residue ellipticity of the mutant was observed, and no defined melting temperature could be determined (Figure 6B), suggesting a structure that was less compact than that of the wild-type enzyme.

Thermal unfolding and refolding from the urea denatured state revealed significant differences between DHFR and G121V-DHFR. DHFR folds via a series of parallel reactions (*53*). Each parallel path proceeds through collapsed burst phase intermediates followed by the formation of a highly fluorescent intermediate. The interconversion between individual folding channels is slow relative to the overall folding, and the mechanism can therefore be described by a four-

state model, in which the initial burst phase intermediates reorganize to form the highly fluorescent intermediates, which contain specific tertiary contacts (*56*). The results presented here indicated that unlike DHFR, which slowly progressed toward the native state, G121V-DHFR was trapped in a state that resembled the highly fluorescent intermediate of the wild-type. The differences in fluorescence intensities observed for the refolding of DHFR and G121V-DHFR implied that there were structural differences between the highly fluorescent states of the wild-type and the folded form of the mutant. For DHFR, stopped-flow CD studies in conjunction with site-directed mutagenesis had demonstrated that Trp 47 and Trp 74 adopted an edge-to-face interaction in the highly fluorescent intermediate as well as in the native protein, suggesting that in the highly fluorescent state the ABD adopted a structure similar to that found in the folded protein (*54*, *57*). The differences in fluorescence between DHFR and G121V-DHFR might therefore indicate a difference in folding of the ABD, in agreement with the 40-fold reduced affinity of the mutant enzyme for NADPH (*27*). However, altered interactions between the M20 and FG loops were also likely to contribute to this reduction in binding affinity, since these loops are involved in the binding of the nicotinamide ring of the cofactor.

It has previously been suggested that the decrease in the reaction rate in G121V-DHFR may arise from the interruption of a network of promoting motions (*13*). The results presented here provide a possible structural basis for this proposal. While the structural changes in G121V-DHFR could not be defined at the atomic level, they appear to contain some rearrangements of the backbone atoms. The reduced activity of the mutant may therefore be explained without invoking long-range coupling of dynamics and catalysis through a network of coupled motions. Rather, it appeared to be based on structural effects of surface mutations on the overall fold of the protein.

ACKNOWLEDGMENT

We thank Giovanni Maglia, Masood H. Javed, and Oliver S. Smart for helpful discussions.

REFERENCES

1. Blakley, R. L. (1984) in *Folates and Pterins* (Blakley, R. L., and Benkovic, S. J., Eds.) pp 191−253, Wiley, New York.
2. Davies, J. F., Delcamp, T. J., Prendergast, N. J., Ashford, V. A., Freisheim, J. H., and Kraut, J. (1990) Crystal Structures of Recombinant Human Dihydrofolate Reductase Complexed with Folate and 5-Deazafolate, *Biochemistry 29*, 9467−9479.
3. McTigue, M. A., Davies, J. F., Kaufman, B. T., and Kraut, J. (1992) Crystal Structure of Chicken Liver Dihydrofolate Reductase Complexed with $NADP^+$ and Biopterin, *Biochemistry 31*, 7264−7273.
4. McTigue, M. A., Davies, J. F., Kaufman, B. T., and Kraut, J. (1993) Crystal Structures of Chicken Liver Dihydrofolate Reductase: Binary ThioNADP$^+$ and Ternary ThioNADP$^+$·Biopterin Complexes, *Biochemistry 32*, 6855−6862.
5. Sawaya, M. R., and Kraut, J. (1997) Loop and subdomain movements in the mechanism of *Escherichia coli* dihydrofolate reductase: Crystallographic evidence, *Biochemistry 36*, 586−603.
6. Osborne, M. J., Schnell, J., Benkovic, S. J., Dyson, H. J., and Wright, P. E. (2001) Backbone dynamics in dihydrofolate reductase complexes: Role of loop flexibility in the catalytic mechanism, *Biochemistry 40*, 9846−9859.
7. Osborne, M. J., Venkitakrishnan, R. P., Dyson, H. J., and Wright, P. E. (2003) Diagnostic chemical shift markers for loop conformation and substrate and cofactor binding in dihydrofolate reductase complexes, *Protein Sci. 12*, 2230−2238.
8. Feeney, J. (2000) NMR studies of ligand binding to dihydrofolate reductase, *Angew. Chem., Int. Ed. 39*, 290−312.
9. Casarotto, M. G., Basran, J., Badii, R., Sze, K. H., and Roberts, G. C. K. (1999) Direct measurement of the pK_a of aspartic acid 26 in *Lactobacillus casei* dihydrofolate reductase: Implications for the catalytic mechanism, *Biochemistry 38*, 8038−8044.
10. Epstein, D. M., Benkovic, S. J., and Wright, P. E. (1995) Dynamics of the Dihydrofolate Reductase Folate Complex: Catalytic Sites and Regions Known to Undergo Conformational Change Exhibit Diverse Dynamical Features, *Biochemistry 34*, 11037−11048.
11. Shrimpton, P., and Allemann, R. K. (2002) Role of water in the catalytic cycle of *E. coli* dihydrofolate reductase, *Protein Sci. 11*, 1442−1451.
12. Shrimpton, P., Mullaney, A., and Allemann, R. K. (2003) Functional role for Tyr 31 in the catalytic cycle of chicken dihydrofolate reductase, *Proteins 51*, 216−223.
13. Watney, J. B., Agarwal, P. K., and Hammes-Schiffer, S. (2003) Effect of mutation on enzyme motion in dihydrofolate reductase, *J. Am. Chem. Soc. 125*, 3745−3750.
14. Agarwal, P. K., Billeter, S. R., Rajagopalan, P. T. R., Benkovic, S. J., and Hammes-Schiffer, S. (2002) Network of coupled promoting motions in enzyme catalysis, *Proc. Natl. Acad. Sci. U.S.A. 99*, 2794−2799.
15. Radkiewicz, J. L., and Brooks, C. L. (2000) Protein dynamics in enzymatic catalysis: Exploration of dihydrofolate reductase, *J. Am. Chem. Soc. 122*, 225−231.
16. Cannon, W. R., Garrison, B. J., and Benkovic, S. J. (1997) Electrostatic characterization of enzyme complexes: Evaluation of the mechanism of catalysis of dihydrofolate reductase, *J. Am. Chem. Soc. 119*, 2386−2395.
17. Leach, A. R., and Klein, T. E. (1995) A Molecular-Dynamics Study of the Inhibition of Chicken Dihydrofolate Reductase by a Phenyl Triazine, *J. Comput. Chem. 16*, 1378−1393.
18. Castillo, R., Andres, J., and Moliner, V. (1999) Catalytic mechanism of dihydrofolate reductase enzyme. A combined quantum-mechanical/molecular-mechanical characterization of transition state structure for the hydride transfer step, *J. Am. Chem. Soc. 121*, 12140−12147.
19. Cummins, P. L., and Gready, J. E. (2000) Combined quantum and molecular mechanics (QM/MM) study of the ionization state of 8-methylpterin substrate bound to dihydrofolate reductase, *J. Phys. Chem. B 104*, 4503−4510.
20. Cummins, P. L., and Gready, J. E. (2000) QM/MM and SCRF studies of the ionization state of 8-methylpterin substrate bound to dihydrofolate reductase: Existence of a low-barrier hydrogen bond, *J. Mol. Graphics 18*, 42−49.
21. Cummins, P. L., and Gready, J. E. (2001) Energetically most likely substrate and active-site protonation sites and pathways in the catalytic mechanism of dihydrofolate reductase, *J. Am. Chem. Soc. 123*, 3418−3428.
22. Agarwal, P. K., Billeter, S. R., and Hammes-Schiffer, S. (2002) Nuclear quantum effects and enzyme dynamics in dihydrofolate reductase catalysis, *J. Phys. Chem. B 106*, 3283−3293.
23. Cummins, P. L., Greatbanks, S. P., Rendell, A. P., and Gready, J. E. (2002) Computational methods for the study of enzymic reaction mechanisms. 1. Application to the hydride transfer step in the catalysis of dihydrofolate reductase, *J. Phys. Chem. B 106*, 9934−9944.
24. Verma, C. S., Caves, L. S. D., Hubbard, R. E., and Roberts, G. C. K. (1997) Domain motions in dihydrofolate reductase: A molecular dynamics study, *J. Mol. Biol. 266*, 776−796.
25. Sham, Y. Y., Ma, B. Y., Tsai, C. J., and Nussinov, R. (2001) Molecular dynamics simulation of *Escherichia coli* dihydrofolate reductase and its protein fragments: Relative stabilities in experiment and simulations, *Protein Sci. 10*, 135−148.
26. Sham, Y. Y., Ma, B. Y., Tsai, C. J., and Nussinov, R. (2002) Thermal unfolding molecular dynamics simulation of *Escherichia coli* dihydrofolate reductase: Thermal stability of protein domains and unfolding pathway, *Proteins 46*, 308−320.
27. Rajagopalan, P. T. R., Lutz, S., and Benkovic, S. J. (2002) Coupling interactions of distal residues enhance dihydrofolate reductase catalysis: Mutational effects on hydride transfer rates, *Biochemistry 41*, 12618−12628.
28. Cameron, C. E., and Benkovic, S. J. (1997) Evidence for a functional role of the dynamics of glycine-121 of *Escherichia coli* dihydrofolate reductase obtained from kinetic analysis of a site-directed mutant, *Biochemistry 36*, 15792−15800.

29. Benkovic, S. J., and Hammes-Schiffer, S. (2003) A perspective on enzyme catalysis, *Science 301*, 1196−1202.
30. Shortle, D. (1992) Mutational Studies of Protein Structures and Their Stabilities, *Q. Rev. Biophys. 25*, 205−250.
31. Rejto, P. A., and Freer, S. T. (1996) Protein conformational substates from X-ray crystallography, *Prog. Biophys. Mol. Biol. 66*, 167−196.
32. Eyal, E., Najmanovich, R., Edelman, M., and Sobolev, V. (2003) Protein side-chain rearrangement in regions of point mutations, *Proteins 50*, 272−282.
33. Eigenbrot, C., Randal, M., and Kossiakoff, A. A. (1992) Structural Effects Induced by Mutagenesis Affected by Crystal Packing Factors: The Structure of a 30−51 Disulfide Mutant of Basic Pancreatic Trypsin Inhibitor, *Proteins 14*, 75−87.
34. Brooks, B. R., Bruccoleri, R. E., Olafson, B. D., States, D. J., Swaminathan, S., and Karplus, M. (1983) Charmm: A Program for Macromolecular Energy Minimization and Dynamics Calculations, *J. Comput. Chem. 4*, 187−217.
35. Lazaridis, T., and Karplus, M. (1999) Effective energy function for proteins in solution, *Proteins 35*, 133−152.
36. Neria, E., Fischer, S., and Karplus, M. (1996) Simulation of activation free energies in molecular systems, *J. Chem. Phys. 105*, 1902−1921.
37. Lazaridis, T., and Karplus, M. (1997) "New view" of protein folding reconciled with the old through multiple unfolding simulations, *Science 278*, 1928−1931.
38. Elber, R., Roitberg, A., Simmerling, C., Goldstein, R., Li, H. Y., Verkhivker, G., Keasar, C., Zhang, J., and Ulitsky, A. (1995) Moil: A Program for Simulations of Macromolecules, *Comput. Phys. Commun. 91*, 159−189.
39. Fierke, C. A., Johnson, K. A., and Benkovic, S. J. (1987) Construction and Evaluation of the Kinetic Scheme Associated with Dihydrofolate Reductase from *Escherichia coli*, *Biochemistry 26*, 4085−4092.
40. Touchette, N. A., Perry, K. M., and Matthews, C. R. (1986) Folding of Dihydrofolate Reductase from *Escherichia coli*, *Biochemistry 25*, 5445−5452.
41. Rod, T. H., Radkiewicz, J. L., and Brooks, C. L. (2003) Correlated motion and the effect of distal mutations in dihydrofolate reductase, *Proc. Natl. Acad. Sci. U.S.A. 100*, 6980−6985.
42. Alonso, D. O. V., and Daggett, V. (2000) Staphylococcal protein A: Unfolding pathways, unfolded states, and differences between the B and E domains, *Proc. Natl. Acad. Sci. U.S.A. 97*, 133−138.
43. Alonso, D. O. V., and Daggett, V. (2001) Simulations and computational analyses of prion protein conformations, *Adv. Protein Chem. 57*, 107−137.
44. Tsai, J., Levitt, M., and Baker, D. (1999) Hierarchy of structure loss in MD simulations of src SH3 domain unfolding, *J. Mol. Biol. 291*, 215−225.
45. Caflisch, A., and Karplus, M. (1995) Acid and Thermal Denaturation of Barnase Investigated by Molecular Dynamics Simulations, *J. Mol. Biol. 252*, 672−708.
46. Sheinerman, F. B., and Brooks, C. L. (1998) Calculations on folding of segment B1 of streptococcal protein G, *J. Mol. Biol. 278*, 439−456.
47. Li, A. J., and Daggett, V. (1996) Identification and characterization of the unfolding transition state of chymotrypsin inhibitor 2 by molecular dynamics simulations, *J. Mol. Biol. 257*, 412−429.
48. Ionescu, R. M., Smith, V. F., O'Neill, J. C., and Matthews, C. R. (2000) Multistate equilibrium unfolding of *Escherichia coli* dihydrofolate reductase: Thermodynamic and spectroscopic description of the native, intermediate, and unfolded ensembles, *Biochemistry 39*, 9540−9550.
49. Ohmae, E., Kurumiya, T., Makino, S., and Gekko, K. (1996) Acid and thermal unfolding of *Escherichia coli* dihydrofolate reductase, *J. Biochem. 120*, 946−953.
50. Gekko, K., Yamagami, K., Kunori, Y., Ichihara, S., Kodama, M., and Iwakura, M. (1993) Effects of Point Mutation in a Flexible Loop on the Stability and Enzymatic Function of *Escherichia coli* Dihydrofolate Reductase, *J. Biochem. 113*, 74−80.
51. Jones, B. E., Beechem, J. M., and Matthews, C. R. (1995) Local and Global Dynamics During the Folding of *Escherichia coli* Dihydrofolate Reductase by Time-Resolved Fluorescence Spectroscopy, *Biochemistry 34*, 1867−1877.
52. Kuwajima, K., Garvey, E. P., Finn, B. E., Matthews, C. R., and Sugai, S. (1991) Transient Intermediates in the Folding of Dihydrofolate Reductase as Detected by Far-Ultraviolet Circular Dichroism Spectroscopy, *Biochemistry 30*, 7693−7703.
53. Jennings, P. A., Finn, B. E., Jones, B. E., and Matthews, C. R. (1993) A Reexamination of the Folding Mechanism of Dihydrofolate Reductase from *Escherichia coli*: Verification and Refinement of a Four-Channel Model, *Biochemistry 32*, 3783−3789.
54. Heidary, D. K., O'Neill, J. C., Roy, M., and Jennings, P. A. (2000) An essential intermediate in the folding of dihydrofolate reductase, *Proc. Natl. Acad. Sci. U.S.A. 97*, 5866−5870.
55. Arai, M., Maki, K., Takahashi, H., and Iwakura, M. (2003) Testing the relationship between foldability and the early folding events of dihydrofolate reductase from *Escherichia coli*, *J. Mol. Biol. 328*, 273−288.
56. Jones, B. E., Jennings, P. A., Pierre, R. A., and Matthews, C. R. (1994) Development of Nonpolar Surfaces in the Folding of *Escherichia coli* Dihydrofolate Reductase Detected by 1-Anilinonaphthalene-8-Sulfonate Binding, *Biochemistry 33*, 15250−15258.
57. Jones, B. E., and Matthews, C. R. (1995) Early Intermediates in the Folding of Dihydrofolate Reductase from *Escherichia coli* Detected by Hydrogen Exchange and NMR, *Protein Sci. 4*, 167−177.

BI036164K